NRIAG Journal of Astronomy and Geophysics (2013) 2, 212–222

National Research Institute of Astronomy and Geophysics

NRIAG Journal of Astronomy and Geophysics

www.elsevier.com/locate/nrjag

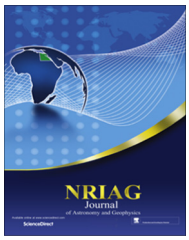

REVIEW ARTICLE

Shallow subsurface structures and geotechnical characteristics of Tal El-Amarna area, middle Egypt

Mostafa Toni [a,*], Ahmed Hosny [a,c], Mohsen M. Attia [b], Awad Hassoup [a], Amr El-Sharkawy [a]

[a] *Seismology Dept., National Research Institute of Astronomy and Geophysics, Helwan, Cairo, Egypt*
[b] *Geology Dept., Faculty of Science, Sohag University, Egypt*
[c] *ICTP North Africa Group for Earthquake and Tsunami Studies (NAGET), Egypt*

Received 10 February 2013; revised 13 June 2013; accepted 31 October 2013
Available online 8 December 2013

KEYWORDS

Seismic refraction;
Noise array;
Frequency–wavenumber;
Dispersion curves;
Geotechnical;
Site classification

Abstract The shallow seismic refraction profiling was carried out at 18 sites in Tal El-Amarna, which is a flat area on the eastern bank of the Nile River, 50 km south of El Minia Governorate, middle Egypt. The collected data are used to estimate the P-wave velocity and to delineate the near-surface ground model beneath the study area. This study is supported by the National Research Institute of Astronomy and Geophysics due to the historical interest of the Tal El-Amarna area as a famous tourist place where there exist many Pharaoh temples and tombs. This area is low seismically active, but it is probably of high vulnerability due to the influence of the local geological conditions on earthquake ground motion, as well as the presence of poor constructions in the absence of various issues such as building designs, quality of building materials, etc.

Another dataset at the study area is obtained by multi-channel passive source (microtremor) measurements, which have been recorded at four arrays. The frequency–wavenumber (*f–k*) method was used to derive the dispersion curves from the raw signals at each array. The resulted dispersion curves were inverted using the neighborhood algorithm to obtain the shear and P-wave velocity models.

The concluded *Vs* and *Vp* values provide a preliminary estimation of the geotechnical parameters and site classification for the shallow soil as they are of great interest in civil engineering applications.

* Corresponding author. Tel.: +20 1111425645; fax: +20 225548020.
E-mail address: m_toni@nriag.sci.eg (M. Toni).
Peer review under responsibility of National Research Institute of Astronomy and Geophysics.

ELSEVIER Production and hosting by Elsevier

2090-9977 © 2013 Production and hosting by Elsevier B.V. on behalf of National Research Institute of Astronomy and Geophysics.
http://dx.doi.org/10.1016/j.nrjag.2013.10.001

Contents

1. Introduction

Tal El-Amarna area is located at the central part of Egypt, southeast of El-Minia Governorate (Fig. 1). It is built on the eastern bank of the Nile River. It was historically known as Akhetaten, which means the horizon of the solar disk. It is very similar to the meaning of Amun Dwelt at Thebes, Ptah at Memphis and other gods at their favored places. Recently, local living people (Bedouins) called this area Tal El-Amarna village. The area is a plain field, separated from the Nile Valley by a strip of palm trees. It is covered mostly by sand and outlined by ruins of temples, palaces and houses that archeologists discovered or are trying to find. Some tourists consider it as the most romantic place they have ever seen, because of the silence and the peaceful beauty that the area has gained through the centuries. Assessment of seismic hazard at this area is therefore interesting for mitigation of the earthquake risk and is here obtained based on estimation of the shallow seismic velocity structures, as well as the site characterization.

In general, El-Minia district is essentially covered with sedimentary rocks, which range in age from Early Eocene to Recent. Recent and Pleistocene sediments appear around the cultivated plain of the Nile valley. The Nile sediments are limited to the Nile valley at the western side of the Tal Al-Amarna village. Tal El-Amarna is located within the Nile basin, which is generally a part of a rocky platform covered mostly by Quaternary deposits. These formations are mainly represented by sand, gravels and recent Nile deposits. However, different types of rock materials having different ages cover most of the area. The Eocene limestone and Quaternary alluvial deposits are also present (Fig. 1). The study area lies between the limestone scarps on the eastern bank and the Nile flood plains on the western side. Different Eocene limestone represents the structural plateau which has irregular outcrops. It is represented by sectors of mountain blocks, which run in NW–SE and NE–SW directions, approximately parallel to the Gulf of Suez and Gulf of Aqaba trends (Yallouze and Knetsch, 1954). Said (1962) described the tectonics of Egypt as a persistent Arabo-Nubia nucleus, of massive rocks, surrounded by stable and unstable shelves. On the basis of his classification, the study area is located in the stable shelf that is composed of rigid foundation of the Pre-Cretaceous rocks; Faulting is common, as a number of horsts and grabens cross this shelf. Also, he stated that most of the stable shelf folds are structures that do not show any lateral loss of the area. These structures are better termed as domes even though some of them may be many times longer than width. The dome's structures are probably due to the uparching of the rigid basement. Therefore, the previously mentioned folds and fault systems are represented in the studied area. Tal El-Amarna area has no fault traces

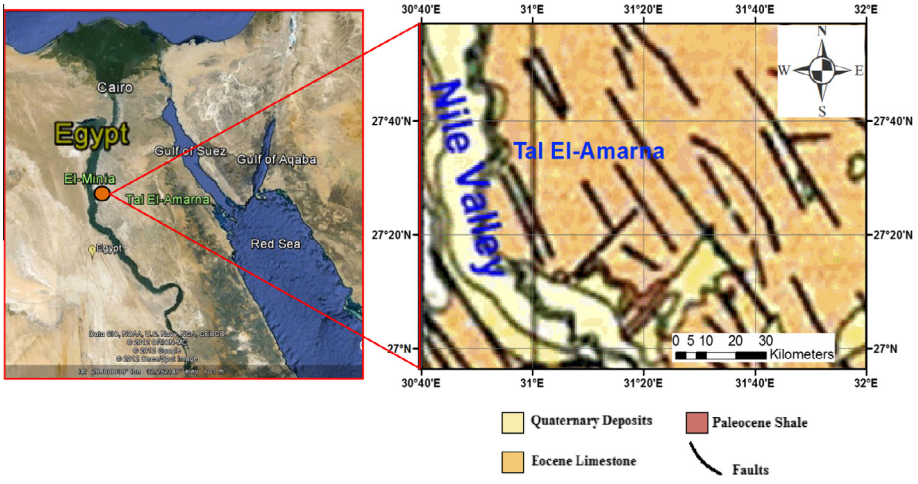

Figure 1 *Left*: Location of the Tal El-Amarna area. *Right:* Geologic map of the Tal El-Amarna from the geologic map of Egypt (EGSMA, 1981).

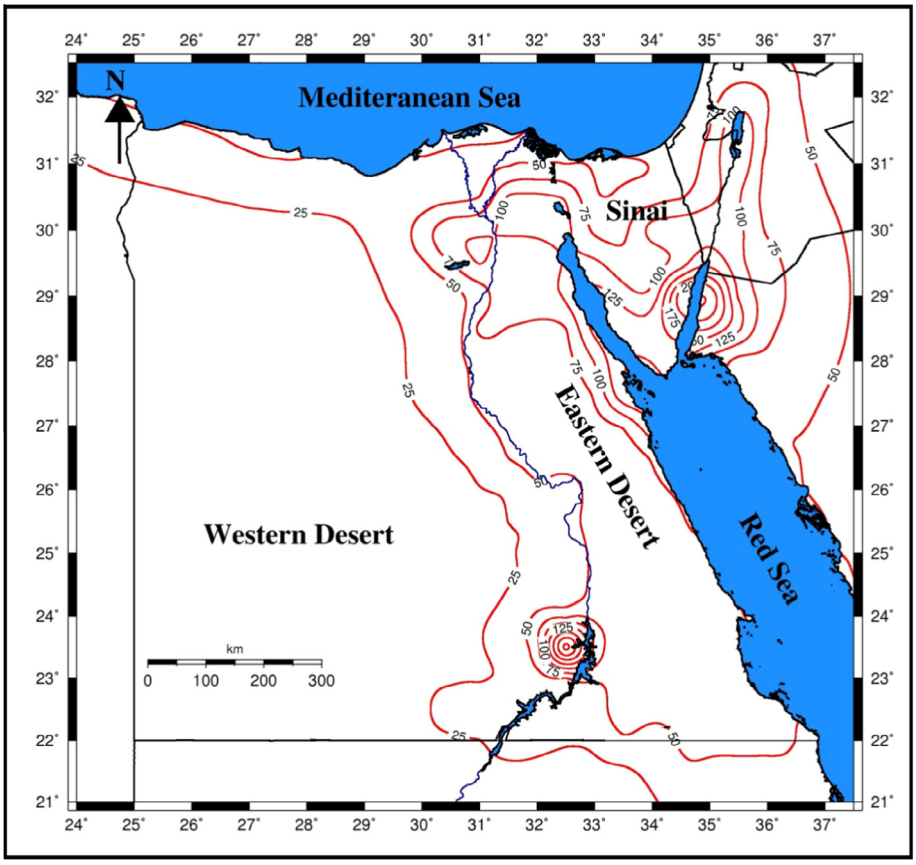

Figure 2 Mean peak ground acceleration (cm/s^2) with 10% probability of exceedance in 50 years (475 years return period) in Egypt (El-Hadidy, 2012).

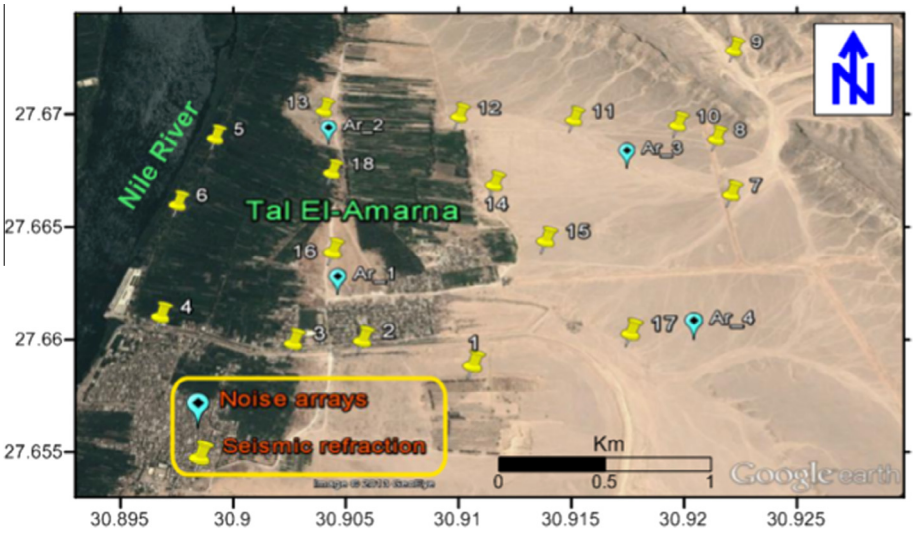

Figure 3 Location of the measured sites in the Tal El-Amarna area.

on the surface. However, some major normal subsurface faults have NW–SE and NE–SW directions (Fig. 1). These faults are encountered in the subsurface below the Quaternary deposits (Said, 1981).

The study area is characterized by low seismic activity but moderate and large size of earthquakes occurring in the Mediterranean and Red Seas, as well as the Gulfs of Suez and Aqaba affect it with intermediate earthquake intensity (e.g., seismic hazard < 100 cm/s^2) (Riad et al., 2000). In a more recent study, the seismic hazard map developed by El-Hadidy (2012) demonstrates that the seismic hazard around the Tal El-Amarna area is 50–75 cm/s^2 (Fig. 2). Although the area of the

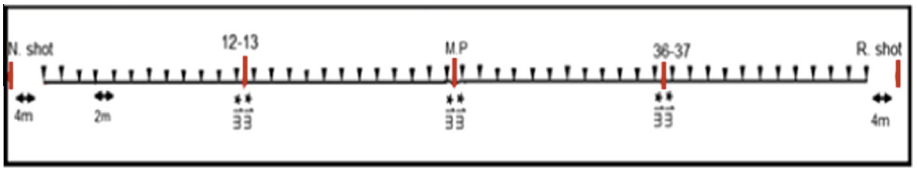

Figure 4 Geometry of seismic refraction profile applied in this study.

Tal El-Amarna is not a place of high seismic hazard, it may be a place of high seismic risk or high probability of seismic losses. This is may be attributed to the influence of near-surface geological conditions on earthquake ground motion and/or the poorly constructed buildings that do not follow anti-earthquake design codes.

2. Field survey

In this study, two types of datasets have been gathered: the shallow seismic refraction profiling and noise array data. The distribution of the investigated sites is shown in (Fig. 3).

The shallow seismic refraction profiling consists of 18 observation sites in which the P-wave velocity is estimated for delineating the near-surface velocity model beneath the study area. The reversed-refraction profile consisting of 48 geophones spaced at 2 m has been here employed. The geophones were firmly coupled to the ground. The refraction survey was carried out using 48-channels signal enhancement seismograph model GEOMETRICS Strata View. A heavy sledgehammer was used as a source of seismic energy. The technique for generating the P-waves is suddenly vertically hitting the ground along the profile of five shots at a distance of 4 m from both ends (normal and reverse shooting), and at the mid-point (between geophones 24 and 25), between geophones 12 and 13, and between geophones 36 and 37 as illustrated in (Fig. 4).

This survey included the application of the multi-channel passive source (noise array) technique which depends on recording ambient noise through an array of sensors for determining the velocity models of shear and P-waves. The reasons of applying this technique in the Tal El-Amarna area are the absence of local seismic activity and to avoid the disturbance for neighboring buildings and Pharaoh temples and tombs. The applications of this method are not limited to earthquake engineering but may also extend to general soil characterization (Wathelet et al., 2008).

Ambient noise is recorded by four arrays (Ar_1, Ar_2, Ar_3, Ar_4) distributed in the study area (Fig. 3). Each array has a maximum aperture of 100 m (except Ar_2 has a maximum aperture of 200 m) and consists of seven seismic stations that record seismic noise simultaneously. The array geometry exhibits triangles or semi-circular shape (one station at the center and six stations at the vertexes of two overlapped triangles) (Fig. 5). For each array, noise signals were recorded at all stations simultaneously with a sampling rate of 100 Hz and 120 min record duration. The measurements were made using a seismic station equipped with data logger model Taurus and three component broadband velocity sensors model Trillium compact (Nanometrics Co.). Taurus incorporates a three channel 24-bit digitizer, GPS receiver and system clock. The guidelines proposed in the European project SESAME (2004) (Site Effects Assessment using Ambient Excitation, http://sesame-fp5.obs.ujf-renoble.fr//SESTechnical Doc.htm) were followed, in order to ensure reliable experimental conditions.

3. Data processing

3.1. Shallow seismic refraction data

In the current study, the recorded seismic signals were processed using SeisImager software package (OYO Corporation, 2004), which is a complete seismic data processing and modeling software. It is based on the time delay and ray tracing methods. The obtained waveforms were analyzed by picking the first arrivals. Arrivals from the second layer were always recognizable on all shot records as first layer arrivals. The arrival times together with the distances between geophones were used in the construction of the travel time–distance (T–D) curves. The resulted T–D curves were analyzed. Then, the 2-D ground models were constructed based on the refracted waves from subsurface interfaces and the P-wave velocities for the subsurface layers were calculated. Examples of the

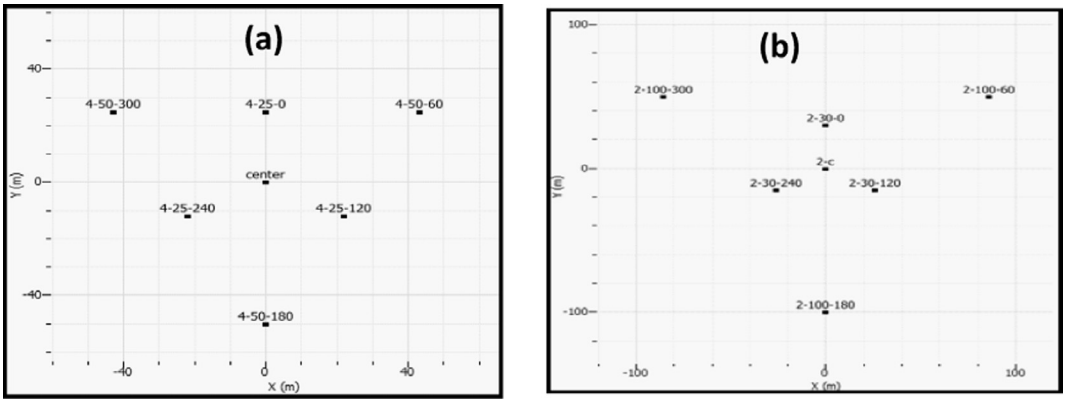

Figure 5 Geometry of Ar_1, Ar_3, Ar_4 (a), and Ar_2 (b).

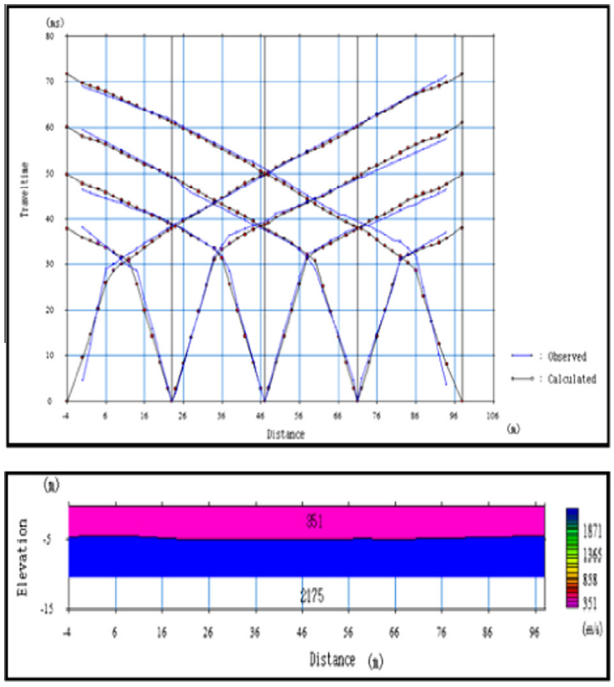

Figure 6 The T–D curve (upper part) and its corresponding depth model (lower part) of site 4 in Fig. 3.

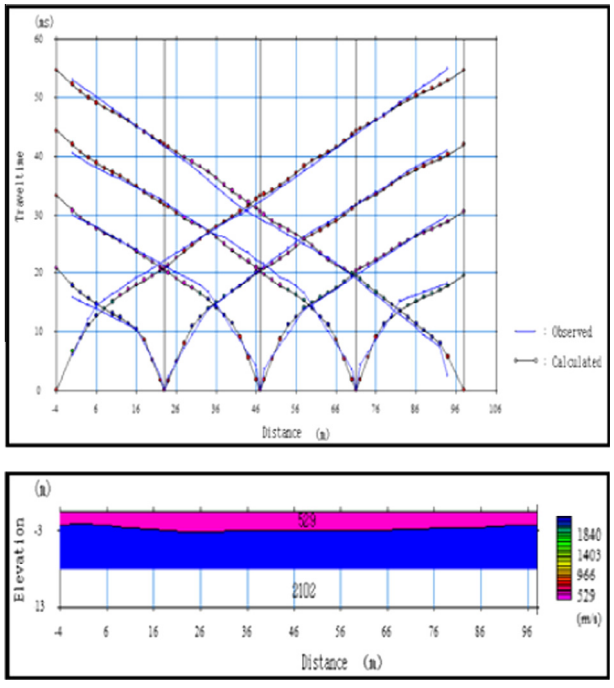

Figure 7 The T–D curve (upper part) and its corresponding depth model (lower part) of site 9 in Fig. 3.

resulted T–D curves and the corresponding depth models are illustrated in Figs. 6 and 7.

3.2. Noise array data

Determination of the shear-wave velocity model based on the noise array data assumes that, the ambient noise is mostly composed of surface waves and the ground structure is approximately horizontally stratified (Tokimatsu, 1997). So, in the one-dimensional heterogeneous media, the surface waves are dispersive and show variation of the apparent velocity as a function of frequency, which in turn controls their penetration depth (Aki and Richards, 2002). This dispersion property can be used to derive *Vs* versus depth through an inversion process (Herrmann, 1994; Wathelet et al., 2004).

Love and Rayleigh modes co-exist on horizontal components, whereas vertical component is affected by Rayleigh-surface waves. The majority of ambient vibration studies focus on the vertical component and on the Rayleigh modes (i.e. Satoh et al., 2001; Wathelet et al., 2004; Picozzi et al., 2005; Kind et al., 2005), although some attempts were made to use Love waves as well (e.g., Chouet et al., 1998; Okada, 2003; Köhler et al., 2007).

Data processing for obtaining the *Vs* profile from noise array measurements is carried out in two main steps: First, deriving the spectral curve (namely, a dispersion curve or auto-correlation curves). Second, the spectral curve is inverted to obtain the *Vs* and eventually the *Vp* vertical profiles. Then, the resolution at depth is intrinsically linked to the wave field spectral amplitudes, as well as to the capabilities of the array of sensors (Wathelet et al., 2008).

In the present work, the processing of noise data is focused only on vertical components and on Rayleigh modes. The analysis was performed using GEOPSY software (http://www.geopsy.org). During the first phase in data analysis, special attention was paid to determine the reliable frequency range of the spectral curve, which depends on the array geometry. For every theoretical array response that takes into account, the real array geometry was computed for that array. The wavenumber limits deduced from the theoretical array response are good estimates of the valid dispersion curve range, as has been also suggested by Wathelet et al. (2008). The next

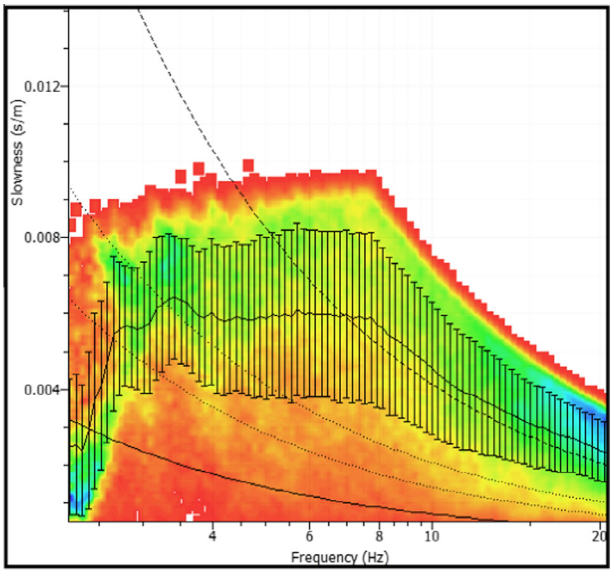

Figure 8 Dispersion curve derived from *f–k* method at Ar_3. The sample mean and sample standard deviation for each frequency histogram are represented by the black line with error bars. The four exponential curves represent constant wavenumber values: $k_{min}/2$ (continuous line), k_{min} (dotted line), $k_{max}/2$ (dashed line) and k_{max} (upper dashed line).

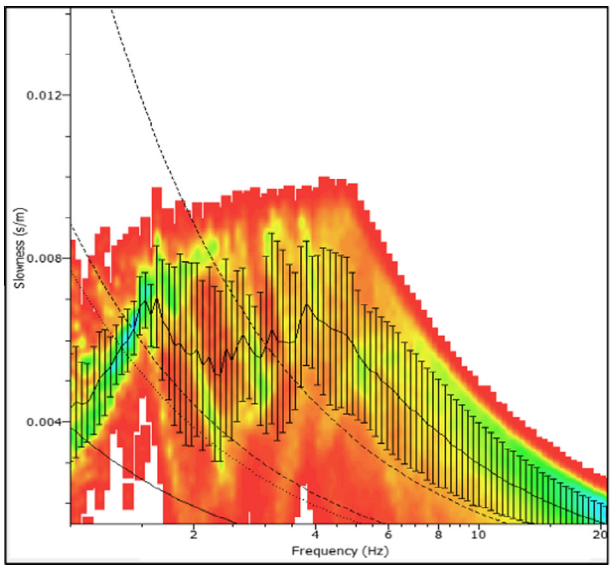

Figure 9 Dispersion curve derived from *f–k* method at Ar_1. The sample mean and sample standard deviation for each frequency histogram are represented by the black line with error bars. The four exponential curves represent constant wavenumber values: $k_{min}/2$ (continuous line), k_{min} (dotted line), $k_{max}/2$ (dashed line) and k_{ma} (upper dashed line).

step is to derive the dispersion curve from noise array signals. The frequency–wavenumber (*f–k*) method was used to derive the dispersion curves from the raw signals. The (*f–k*) analysis assumes plane waves to travel across array of sensors laid out at the surface. Considering a wave with frequency *f*, a direction of propagation and a velocity (or equivalently k_x and k_y, wavenumbers along *X* and *Y* horizontal axis, respectively), the relative arrival times are calculated at all sensor locations and the phases are shifted according to the time delays. The array output is calculated by the summation of shifted signals in the frequency domain. If the waves travel with a given direction and velocity, all contributions will stack constructively, resulting in a high array output (usually called the beam power, Capon, 1969). The location of the maximum beam power in the plane (k_x, k_y) provides an estimate of the velocity and of the azimuth of the traveling waves across the array. During this stage in data analysis the following steps were applied on the raw signals:

- The recorded waveforms are divided into short time windows. The length of which depends on the considered frequency band. Pre-processing methods may be used to reject transients or saturated signals (Bard, 1998; Wathelet, 2005).
- A Fourier transform is calculated for the signal of each sensor after a proper cutting of time windows.
- Application of cosine taper.
- The frequency–wavenumber transformation itself is calculated in the frequency domain on the cut signals.

Examples of the dispersion curves and theoretical array response obtained in this study are shown in Figs. 8 and 9.

At the final stage, the resulted dispersion curves are inverted using the neighborhood algorithm (Sambridge, 1999; Wathelet, 2008) to obtain the one-dimensional *Vs* and eventually *Vp* velocity models at the measured sites.

4. Results and interpretations

Table 1 summarizes the results of shallow seismic refraction survey at the Tal El-Amarna area. The obtained depth models of all profiles revealed surface layer overlays of the limestone bedrock. The thickness of this layer varies from 1–6 m. By spatial interpolation of the resulted P-wave velocities at all measured sites, the maps that show the distributions of *Vp* in the surface layer and bedrock are produced and shown in Figs. 10 and 11, respectively. The P-wave velocity in the surface layer generally decreases from northeast to southwest as illustrated in (Fig. 10). This is can be interpreted as follows: Below the limestone outcrops in northeastern part of the study area, the surficial layer consists of cohesive deposits that graded to agricultural soil toward the Nile River in the southwest. On

Table 1 Results of shallow seismic refraction survey at the Tal El-Amarna area.

Profile no.	Coordinates		Surficial layer		2nd Layer
	Lat.	Long.	*Vp* (m/s)	Thickness (m)	*Vp* (m/s)
1	27.6575	30.9099	466	3	1721
2	27.6585	30.9058	487	2–3	1966
3	27.6584	30.9032	366	4	2156
4	27.6595	30.8981	329	5	1914
5	27.6677	30.8996	303	5	2155
6	27.6645	30.8983	351	5	2175
7	27.6649	30.9206	601	2–3	1629
8	27.6676	30.9204	673	1–2	1367
9	27.6722	30.9218	529	3	2101
10	27.6683	30.9189	549	3–4	1332
11	27.6686	30.9146	530	2–3	1019
12	27.6688	30.9098	573	2–4	1209
13	27.6691	30.9041	561	3–4	1864
14	27.6654	30.9111	466	2	1389
15	27.6628	30.9130	398	2	1352
16	27.6623	30.9046	593	3–5	1707
17	27.6588	30.9159	525	3–6	1349
18	27.666	30.9045	373	3	1892

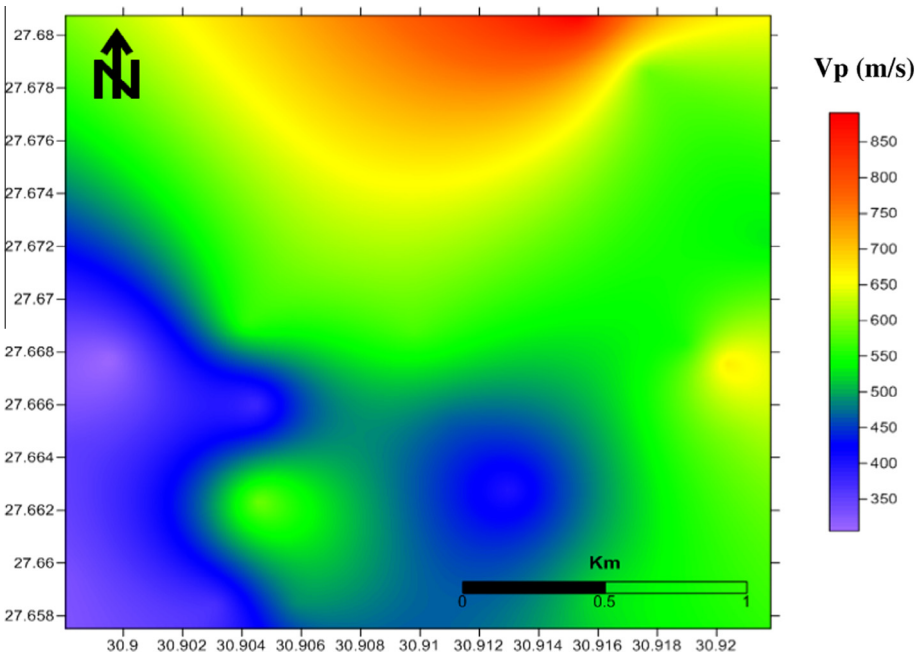

Figure 10 Distribution of P-wave velocity in the surface layer.

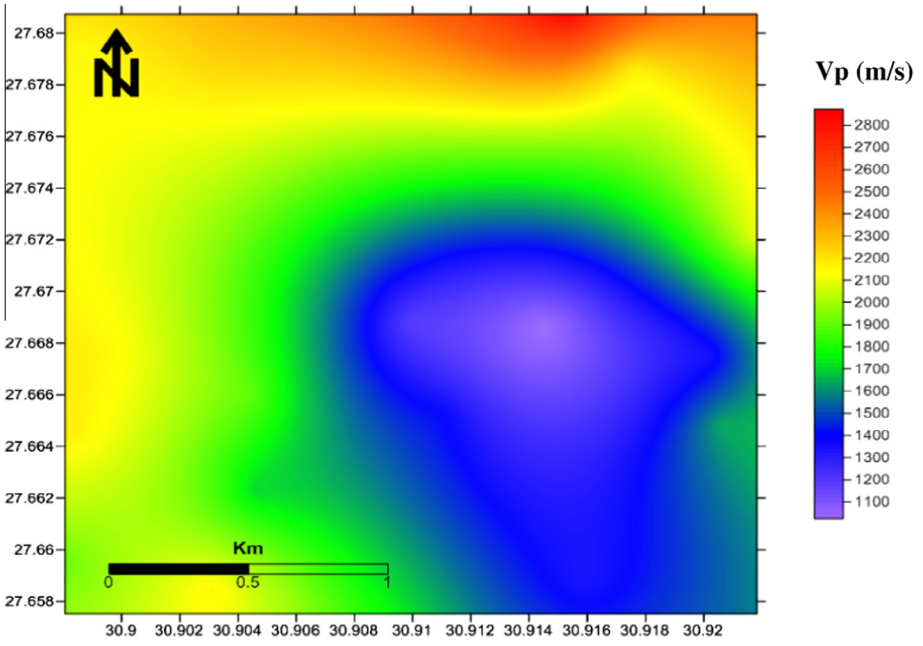

Figure 11 Distribution of P-wave velocity in the bedrock.

the other hand, the velocity distribution of the bedrock (Fig. 11) demonstrates that the *Vp* generally increases from south to north in the study area. This is consistent with the geological setting of the studied area whereas the valley becomes narrow and the limestone outcrops appear more close to the Nile River in the north direction. Also, the southwestern part at the study area shows a zone of low P-wave velocity (Fig. 11). This zone is characterized by low topography and is occupied by fills during the construction of the roads that link the village to the temples and tombs in the southwest.

The depth-velocity models obtained by inversion of the dispersion curves of arrays (Ar_1, Ar_2, Ar_3, and Ar_4) are shown in Fig. 12. The velocity model considered in this work is the model of lowest misfit value that has been indicated by a black line (see Fig. 12). As illustrated in Fig. 12, the results show a good correlation between the measured and inverted dispersion curves. The results exhibit no large variation in seismic velocities within the study area. Only *Vp* model at site Ar_4 shows low velocities relative to that of other sites (see Fig. 12).This is compatible with the results deduced from the seismic refraction profiling at this zone (Fig. 11).

The resulted velocity models show that the studied area is characterized by relatively high *Vp*/*Vs* ratio (~2). This is

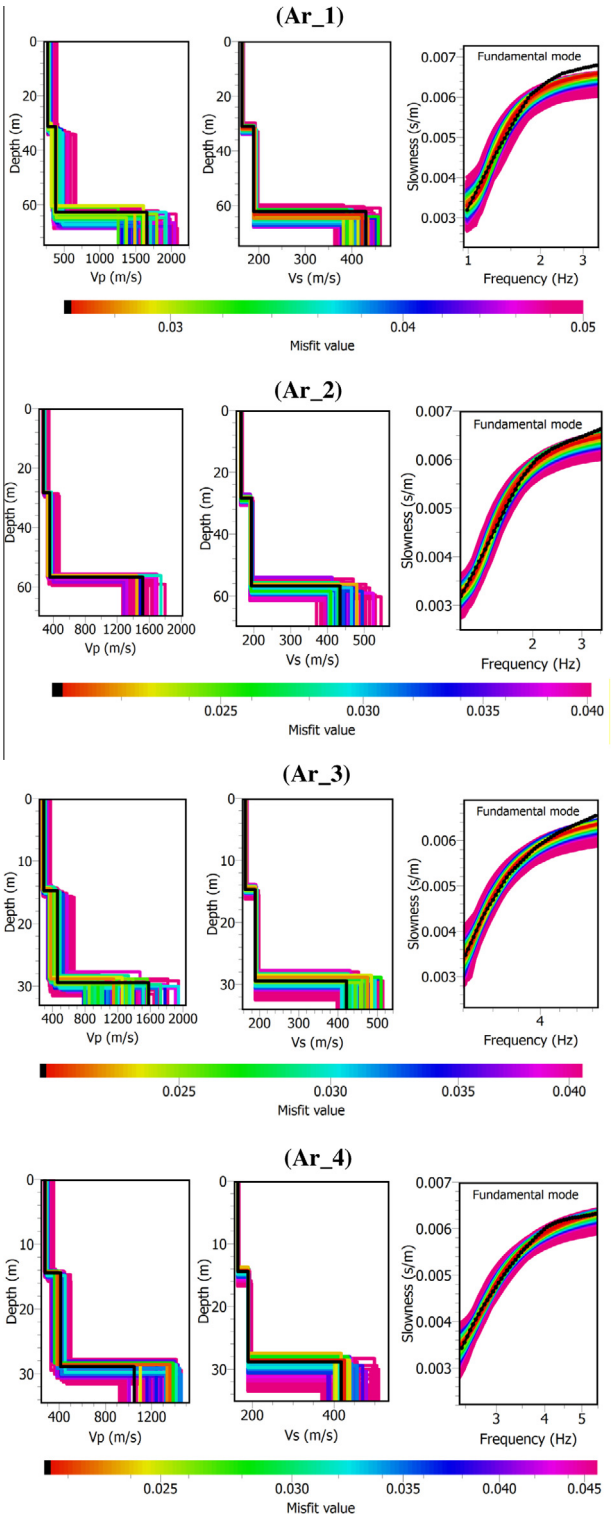

Figure 12 Depth-velocity models of Ar_1, Ar_2, Ar_3, and Ar_4, left: *Vp*; middle: *Vs*; right: dispersion curves of Rayeigh waves, inverted (colors) and measured (black).

may be related to the effect of groundwater in the saturated zone of the Nile River which leads to reduce the shear-wave velocity.

In this article, we also estimated the geotechnical parameters and dynamic characteristics for the near surface soil (up to 30 m depth) at the investigated area. The definitions of these parameters are explained in Table 2. These estimations were performed for some sites that represent a good coverage to the studied area (i.e., sites of profiles 6, 10, 13, 15, 16, 17 in Fig. 3). The calculation of these parameters depends on the propagation of seismic waves (*Vp* & *Vs*) through the soil materials. The *Vp* values used in this calculation were extracted

Table 2 Definitions of geotechnical parameters and dynamic characteristics applied in this study.

Parameter	Relationship	References
Density (ρ)	$\rho = aVp^{1/4}$ a is a constant equals 0.31 when the density is given in g/cm^3 and Vp is in m/s	Nafe and Darke (1963) and Gardner et al. (1974)
Poisson's ratio (σ)	$\sigma = ((V_P/V_S)^2 - 2)/(2(V_P/V_S)^2 - 2)$	Gretener (2003)
Rigidity modulus (μ)	$\mu = \rho V_S^2$	Sharma (1978)
Young's modulus (E)	$E = 2(1 + 2\sigma)\mu$	Lowrie (1997)
Bulk modulus (λ)	$\lambda = \frac{E}{3(1-2\sigma)}$	Abd El-Rahman (1989) and Mott et al. (2008)
Material index (M_i)	$M_i = (1 - 4\sigma)$	Abd El-Rahman (1989)
Concentration index (C_i)	$C_i = (3 - 4\alpha)/(1 - 2\alpha)$ α is the velocity squared ratio $\alpha = (Vs^2/Vp^2)$	Abd El-Rahman (1989)
Stress ratio (S_i)	$S_i = SH/SV = 1 - 2(V_S^2/V_P^2)$ SV is the vertical stress and SH is the horizontal stress at a certain depth	Thomson (1986)
Ultimate bearing capacity (Q_{ult})	$LogQ_{ult} = 2.932\ (\log V_S - 1.45)$	Bowles (1984) and Abd El-Rahman et al. (1992)

Table 3 Site classification scheme of NEHRP provisions (2003).

Site class	Site description	Parameters	
		$V_{S,\ 30}$ (m/s)	N_{SPT}
A	Hard rock	> 1500	–
B	Rock	760–1500	–
C	Very dense soil and soft rock	360–760	> 50
D	Stiff soils	180–360	15–50
E	Soft soils, profile with more than 10 ft (3 m) of soft clay	180	< 15
F	Soils requiring site specific evaluations	–	–

Table 4 Geotechnical parameters and site classes (up to 30 m depth) for selected sites in the Tal El-Amarna area.

Parameter/profile	Profile 6	Profile 10	Profile 13	Profile 15	Profile 16	Profile 17
Vp (m/s)	1450	1250	1500	1100	1450	1200
Vs (m/s) calculated	828	625	857	550	828	600
Site class	B	C	B	C	B	C
Density (ρ) gm/cm^3	1.9	1.8	1.9	1.78	1.9	1.8
Poisson's ratio (σ)	0.26	0.33	0.25	0.33	0.26	0.33
Rigidity modulus (μ) Dyn/cm^2	1.31E + 10	7.2E + 09	1.41E + 10	5.4E + 09	1.31E + 10	6.5E + 09
Young's modulus (E) Dyn/cm^2	3.30E + 10	1.92E + 10	3.56E + 10	1.44E + 10	3.30E + 10	1.7E + 10
Bulk modulus (λ) Dyn/cm^2	2.27E + 10	1.92E + 10	2.45E + 10	1.44E + 10	2.27E + 10	1.7E + 10
Material index (M_i)	−0.032	−0.33	−0.03	−0.33	−0.03	−0.033
Concentration index (C_i)	4.87	4.0	4.88	4.0	4.87	4.0
Stress ratio (S_i)	0.34	0.5	0.34	0.5	0.34	0.5
Ultimate bearing capacity (Q_{ult}) kg/cm^2	20.1	8.8	22.3	6.0	20.1	7.8

from the results of seismic refraction profiling, since this technique provides reliable information about seismic velocities and characteristics of interfaces in the shallow subsurface layers. The shear-wave velocities were calculated from the Vp value at the same seismic refraction profile using the Vp/Vs ratio of the nearest noise array site.

The site classification scheme of NEHRP provisions (National Earthquake Hazards Reduction Program, 2003), which is based on the average shear-wave velocity in the upper 30 m of the soil column (Vs_{30}), is employed in preliminary site classification for the investigated area (Table 3). This application in the study area suggests two site classes B and C of the NEHRP provisions scheme. Class B corresponds to zone of limestone rock sites in the eastern part of the study area. While Class C is mainly prevailing in areas close to the Nile bank on the west. The calculated geotechnical parameters and site classes for the selected sites in the Tal El-Amarna area are listed in Tables 4.

5. Conclusions

This work is carried out and supported by the National Research Institute of Astronomy and Geophysics in the Tal El-Amarna area due to its historical interest as a tourist place aiming to investigate the velocity models (Vp & Vs) and to estimate dynamic characteristics for the shallow subsurface layers. The shallow seismic refraction profiling is carried out at 18

profiles in order to estimate the P-wave velocity and to delineate the near-surface ground model beneath the Tal El-Amarna area. The resulted depth models of all refraction profiles revealed surface layer overlays directly at the limestone bedrock. The ambient noise is recorded by four arrays at the study area to infer the velocity models (Vs and Vp). The frequency–wavenumber (f–k) method was used to derive the dispersion curves that were inverted using the neighborhood algorithm. The one-dimensional Vs and eventually Vp velocity models were obtained at the measured sites. The estimated values of Vs and Vp were used in a preliminary estimation of the dynamic characteristics for the near-surface soil (up to 30 m depth), which are very important in construction purposes. Also, the site classification is also performed to the Tal El-Amarna area by applying the classification scheme of NEHRP provisions. The average shear-wave velocity in the upper 30 m of the soil column (Vs_{30}) was used in this preliminary classification.

In summary, the following conclusions have been obtained:

(1) Shallow seismic refraction profiling gives reliable information on seismic velocities (Vp) and characteristics of the interfaces at the near-surface layers at the Tal El-Amarna area.
(2) Recording ambient noise through an array of sensors is an effective tool for in situ measurements of seismic velocity structure. The procedure is suitable in the investigation of velocity structures with low cost applications in comparing with other techniques.
(3) According to the NEHRP provisions scheme, the area of the Tal El-Amarna is preliminarily classified into two site classes, (B and C).
(4) The area of investigation requires more seismological, geotechnical, and tectonic studies in order to explain adequately the features of ground motion excitation and propagation.

Acknowledgments

This study is supported by the National Research Institute of Astronomy and Geophysics by good facilities during fieldwork and data processing. We thank the staff of the Egyptian Antiquities Organization for their kind help during the fieldwork. The authors are very grateful to the anonymous reviews.

References

Abd El-Rahman, M., 1989. Evaluation of the kinetic moduli of the surface materials and application to engineering geologic maps at Ma'Barrisabah area (Dhamar province). North. Yemen. Egypt. J. Geol. 33 (1–2), 229–250.

Abd El-Rahman, M., Setto, I., and El-Werr, A., 1992. Inferring mechanical properties of the foundation materials at the 2nd Industrial zone city, from geophysical measurements E.G.S. Proc. of the 10th Ann. Meet, pp. 50–61.

Aki, K., Richards, P.G., 2002. Quantitative Seismology, Second ed. University Science Books.

Bard, P.-Y., 1998. Microtremor measurements: A tool for site effect estimation. Second International Symposium on the Effects of Surface Geology on Seismic Motion, Irikura, Kudo Okada & Sasatani (Eds.), Balkema, pp. 1251–1279.

Bowles, J.E., 1984. Physical and Geotechnical Properties of Soils. Mc Grew- Hill, London.

Capon, J., 1969. High-resolution frequency–wavenumber spectrum analysis. Proc. IEEE 57, 1408–1418.

Chouet, B., De Luca, G., Milana, G., Dawson, P., Martini, M., Scarpa, R., 1998. Shallow velocity structure of Stromboli Volcano, Italy, derived from small-aperture array measurements of strombolian tremor. Bull. Seism. Soc. Am. 88, 653–666.

EGSMA, 1981. Geologic map of Egypt, Scale 1:2,000,000, Egyptian Geological Survey and Mining Authority.

El-Hadidy, M.S., 2012. Seismotectonics and seismic hazard studies in and around Egypt. PhD thesis, Faculty of Science, Ain Shams University, Egypt.

Gardner, G.H.F., Gardner, L.W., Gregory, A.R., 1974. Formation velocity and density – the diagnostic basics for stratigraphic traps. Geophysics 39, 770–780.

Gretener, P., 2003. Summary of the Poisson's Ratio Debate 1990–2003. Feature Article, CSEG recorder, September 2003, pp. 44–45.

Herrmann, R.B., 1994. In: Computer Programs in Seismology, vol. IV. St. Louis University.

Kind, F., Fäh, D., Giardini, D., 2005. Array measurements of S-wave velocities from ambient vibrations. Geophys. J. Int. 160, 114–126.

Köhler, A., Ohrnberger, M., Scherbaum, F., Wathelet, M., Cornou, C., 2007. Assessing the reliability of the modified three-component spatial autocorrelation technique. Geophys. J. Int. 168, 779–796.

Lowrie, W., 1997. Fundamentals of Geophysics. Cambridge University Press, p. 354.

Mott, P.H., Dorgan1, J.R., Roland, C.M., 2008. The bulk modulus and Poisson's ratio of "incompressible" materials. J. Sound Vibrat. 312, 572–575.

Nafe, J.E., Darke, C.L., 1963. Physics properties of marine sediments. In: Hill, M.N. (Ed.), . In: The Sea, vol. 3. Interscience Publishers, New York, pp. 794–815.

NEHRP, 2003. Recommended provisions for seismic regulations for New Buildings and Other Structures. Building Seismic Safety Council (BSSC) for the Federal Emergency Management Agency (FEMA 450). Washington, Part 1: Provisions.

Okada, H., 2003. The microseismic survey method: Society of Exploration Geophysicists of Japan. Translated by Koya Suto. In: Geophysical Monograph Series No. 12. Society of Exploration Geophysicists.

OYO Corporation, 2004. Annual Report, www.oyo.co.jp.

Picozzi, M., Parolai, S., Richwalski, S.M., 2005. Joint inversion of H/V ratios and dispersion curves from seismic noise: estimating the S-wave velocity of bedrock. Geophys. Res. Lett. 32, L11308. http://dx.doi.org/10.1029/2005GL0228 78.

Riad, S., Ghalib, M., El-Difrawy, M.A., Gamal, M., 2000. Probabilistic seismic hazard assessment in Egypt. Ann. Geol. Surv. Egypt. XXIII: p. 851.

Said, R., 1962. The Geology of Egypt. ElSevier Publ. Co., Amsterdam, NY, p. 377.

Said, R., 1981. Geological Evaluation of the Nile. Springer-Verlag, Berlin, NY, 51p.

Sambridge, M., 1999. Geophysical inversion with a neighbourhood algorithm: I. Searching a parameter space. Geophys. J. Int. 138, 479–494.

Satoh, T., Kawase, H., Matsushima, S.I., 2001. Estimation of S-wave velocity structures in and around the Sendai Basin, Japan, using array records of microtremors. Bull. Seism. Soc. Am. 91, 206–218.

SESAME, 2004. Site effects assessment using ambient excitations: guidelines for the implementation of the H/V spectral ratio technique on ambient vibrations measurements, processing and interpretation. European research project, WP12 – Deliverable D23.12, December 2004.

Sharma, P.V., 1978. Geophysical Methods in Geology, Second ed. Elsevier, Oxford, New York.

Thomson, L., 1986. Weak elastic anisotropy. Geophys. Prospect. 51, 1954–1966.

Tokimatsu, K., 1997. Geotechnical site characterization using surface waves. In: Ishihara (ed.), Proc. 1st Intl. Conf. Earthquake Geotechnical Engineering, vol. 3. Balkema, pp. 1333–1368.

Wathelet, M., Jongmans, D., Ohrnberger, M., 2004. Surface wave inversion using a direct search algorithm and its application to ambient vibration measurements. Near Surf. Geophys. 2, 211–221.

Wathelet, M., 2005. Array recordings of ambient vibrations: surface-wave inversion. PhD thesis, Université de Liège, Belgium.

Wathelet, M., Jongmans, D., Ohrnberger, M., Bonnefoy-Claudet, S., 2008. Array performances for ambient vibrations on a shallow structure and consequences over Vs inversion. J. Seismol. 12, 1–19.

Wathelet, M., 2008. An improved neighborhood algorithm: parameter conditions and dynamic scaling. Geophys. Res. Lett. 35. http://dx.doi.org/10.1029/2008 GL033256, L09301.

Yallouze, M., Knetsch, G., 1954. Linear structures in and around the Nile basin. Bull. Soc. Geograph. 27, 153–207.